



Lansoprazole, a cure-four, enables perovskite solar cells efficiency exceeding 24%

Xiaobing Wang^a, Weihai Sun^{a,*}, Yongguang Tu^b, Qiu Xiong^c, Guodong Li^a, Zeyu Song^a, Ying Wang^a, Yitian Du^a, Qi Chen^a, Chunyan Deng^a, Zhang Lan^a, Peng Gao^c, Jihuai Wu^{a,*}

^a Engineering Research Centre of Environment-Friendly Functional Materials, Ministry of Education, Fujian Engineering Research Centre of Green Functional Materials, Huaqiao University, Xiamen 361021, China

^b Frontiers Science Center for Flexible Electronics, Northwestern Polytechnical University, Xi'an 710072, Shaanxi, China

^c Fujian Institute of Research on Structure Matter, Chinese Academy of Sciences, CAS, Xiamen 361021, China



ARTICLE INFO

Keywords:

Perovskite solar cells
Additive engineering
Lansoprazole
Defect passivation
Energy level alignment

ABSTRACT

The practical applications of organic-inorganic hybrid metal halide-based perovskite solar cells (PSCs), as the fastest growing photovoltaic devices, are limited by the further improvement of their stability and performance. Additive engineering is considered as a hopeful strategy to alleviate these issues. Herein, Lansoprazole (Lanz), as a multifunctional additive, has four effects for ameliorating the stability and performance of PSCs. The strong hydrophobic trifluoromethyl group on Lanz can cover atop of perovskite to build a moisture-oxygen-barrier; The high electron-donating sulfinyl moiety on Lanz can provide lone electron pair to lead ions to passivate defects; The modification of Lanz can adjust Fermi-level of perovskite and optimize the energy match of functional layers; The introduction of Lanz can moderate the growth rate of perovskite, improve crystal quality and reduce grain boundaries and defects. Consequently, the Lanz-modified device achieves an excellent PCE of 24.05% compared to the pristine device (PCE of 21.91%). Meanwhile the modified device possesses excellent environmental and operational stability that maintains 84% of its initial PCE under continuous irradiation for 500 h.

1. Introduction

As a rising star for next-generation photovoltaic technology, organic-inorganic hybrid metal halide-based perovskite solar cells (PSCs) has been experiencing an increasing surge in the research activities. Up to now so far, the certified power conversion efficiency (PCE) of PSC has reached 25.7% [1], which is close to seven times of its initial value (3.8%) reported in 2009 [2]. The astonishing achievement for PSCs is ascribed to the perovskite outstanding opto-electronic attributes and cost-effective fabrication process [3-7]. Nevertheless, the PSCs suffer from their susceptibility to deteriorate under exposure to the environmental stimuli (e.g., light illumination, humidity and thermal stress), which requires to be tackled before the realization of commercial application [8-10].

In the process of making perovskite (PVSK) absorption layer by frequently used solution method, numerous defects generate on the surface and in the body of perovskite owing to the low formation energy and uncontrollable crystallization process [11]. These defects (including interstitial, vacancy and substitution) could not only act as non-radiative

recombination centers, but also become vulnerable to the oxygen and moisture, causing the serious degradation in both stability and performance of PSCs [12]. In addition, these defects affect the migration of ions under applied voltage, resulting in serious hysteresis effect of PSCs [13]. Therefore, it is very crucial to cure these defects for achieving high-performance and stable PSCs.

Additive engineering is considered to be one of most simple and effective strategy to mitigate and passivate these defects [14]. Various additives with different functional groups including carboxyl ($-COOH$), amine ($-NH_2$), halide ($-X$), hydroxyl ($-OH$) and so forth have been attempted [15-18]. Among them, some biological molecule additives have aroused special attention [19-23]. For instance, a biological molecule (caffeine, 1,3,7-trimethylxanthine), was introduced into PVSK films, which could retard the growth of PVSK crystal and the formation of defects through a strong interaction with Pb^{2+} ions using its carboxyl groups [22]. Similarly, Hou et al. utilized a sesquiterpene lactone (artemisinin), a famous drug molecule against malaria, to establish a “PVSK/PVSK” bilayer structure in the PVSK film, which up-shifts the Fermi level of PVSK layer, leading to an effective electron blocking

* Corresponding authors.

E-mail addresses: sunweihai@hqu.edu.cn (W. Sun), jhwu@hqu.edu.cn (J. Wu).

behavior and a higher open-circuit voltage (V_{OC}) in the modified devices [23,24]. Although biomolecules have achieved some effects as additives, it is still promising to search for novel multifunctional medicine molecules to realize high-performance and stable PSCs.

As a medicine, lansoprazole (Lanz, $C_{16}H_{14}F_3N_3O_2S$) can cure gastritis [25–27]. As a multifunctional molecule, lansoprazole has four effects at least for improving the stability and performance of PSCs. An strong hydrogen bond between the trifluoromethyl ($-CF_3$) group on Lanz and FA^+ on perovskite can be formed to consolidate the crystal structure of PVK, and build a moisture and oxygen barrier atop the PVK film. The sulfinyl ($>S = O$) moiety on Lanz can coordinate with uncoordinated Pb^{2+} ions, which minimize the defects on the interface and in the body of PVK films, thus minimizing carrier nonradiative recombination loss and improving the performance of PSCs. The introduction of Lanz could adjust the Fermi-level of PVK film and cause surface band-bending effect, thereby optimize the energy match between functional layers, which unhinders the separation, extraction and transport of carriers. The introduction of Lanz retards the crystal growth rate of PVK, ameliorates the crystal quality, reduces grain boundaries and defects, and contributes to the enhancement of performance. Consequently, the maximum PCE of device is effectively improved from 21.91% to 24.05% by the multifunctional Lanz additive. Moreover, the unencapsulated Lanz-modified PSC sustains 84% of its original efficiency under a continuous irradiation (100 mW cm^{-2}) for 500 h, indicating an excellent device stability.

2. Results and discussion

Fig. 1a demonstrates the molecular structures of lansoprazole (Lanz). Density function theory (DFT) calculations were carried out and the simulated electrostatic potential surface (EPS) image is shown in **Fig. 1b** to figuratively express the molecular charge distribution in 3D of Lanz [28,29]. It can be seen that the reddest point appears at the sulfinyl moiety ($>S = O$) position, indicating that the group has the strongest electron donating ability can provide chemical chelation site for

unsaturated Pb^{2+} in the PVK film [30]. The interaction of Lanz with both surface and interior of PVK films is schematically illustrated in **Fig. 1c**. The sulfinyl group with higher electron density in Lanz could provide lone electron pairs to the empty orbit of Pb^{2+} , effectively passivate the defects of Pb^{2+} , and reduce non-radiative recombination centers. On the other hand, the trifluoromethyl ($-CF_3$) group with excellent hydrophobicity covered on the surface of PVK would increase the moisture resistance of PVK film, ultimately the environmental stability of PSCs.

Fig. 1d and **1g** show the top-view SEM images of the pristine and Lanz-modified PVK films, respectively. Clearly, the Lanz-modified PVK film shows a uniform morphology with larger grain size ($0.91 \mu\text{m}$) compared to the pristine one ($0.75 \mu\text{m}$). Furthermore, the roughness of the PVK films is evaluated by using Atomic Force Microscopy (AFM), and the related result is shown in **Fig. 1e** and **1h**. The roughness of the PVK films is reduced from 23.9 nm to 19.5 nm after Lanz modification. The smoother surface, uniform and enlarged grain may be due to that the introduction of Lanz in the precursor solution retards the crystal growth rate and improves the quality of perovskite crystal, and reduces the grain boundaries, which contribute to reduce interfacial defects and non-radiative recombination, enhance the stability and performance of the devices [31,32]. To investigate the effect of Lanz on the PVK crystal growth rate, the morphology evolution of PVK film during the heat-treatment are shown in **Fig. S1**. It can be observed that the PVK film with Lanz turns black slower than the pristine PVK film, suggesting that the PVK crystal growth rate is retarded by the introduction of Lanz.

The cross-sectional SEM images of the device is presented in **Fig. S2** of Supporting Information (SI), it can be observed clearly the device architecture of FTO/SnO₂/PVK/spiro-OMeTAD/Au, and the introduction of Lanz does not change the longitudinal distribution of the crystal of PVK. The crystalline phase of PVK films was evaluated by measuring X-ray diffraction (XRD), and the results are shown in **Fig. S3**. As can be seen, the diffraction intensity of (110) plane of PVK is significantly improved after Lanz modification. Besides, a narrower full width at half maximum (FWHM) of the (110) phase of Lanz-doped PVK

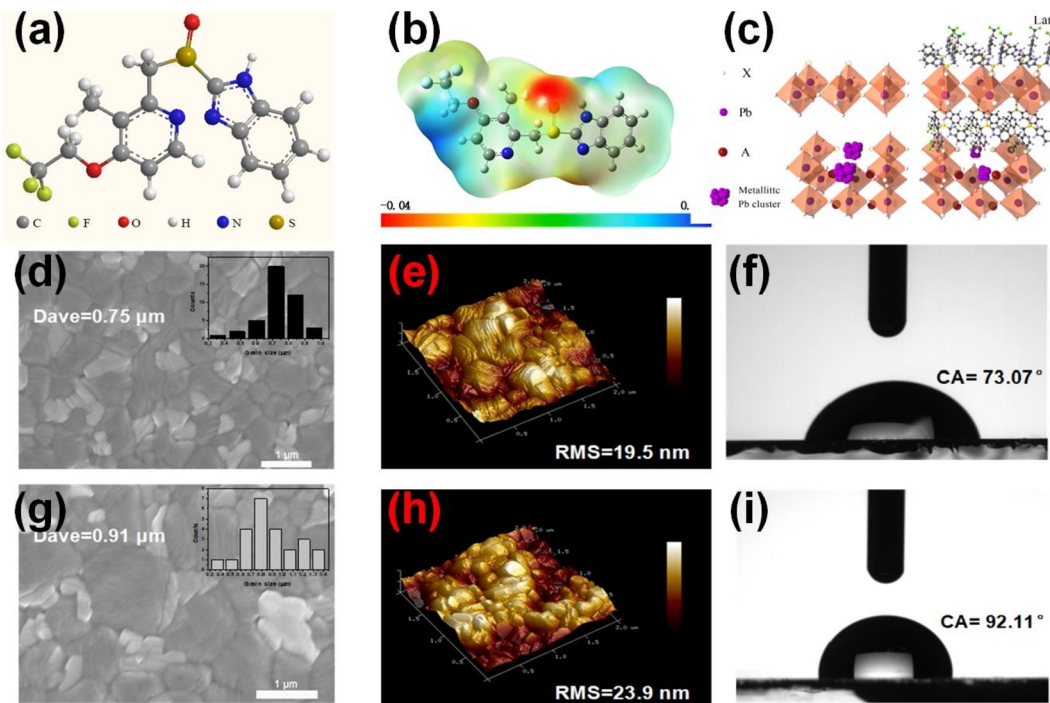


Fig. 1. (a) Molecular structure of lansoprazole (Lanz). (b) Simulated electrostatic potential surface (EPS) image by density functional theory (DFT). (c) Schematic illustration of Lanz interaction with passivated the surface and bulk of PVK layers. Top-view SEM images (insets: grain size distributions), 3D AFM image, and water contact angles of pristine perovskite film (d, e, f) and Lanz-modified perovskite film (g, h, i).

film could be observed in comparison with that of pristine one, implying that a highly crystalline PVK film could be obtained through the introduction of Lanz into the PVK precursor solution, this result is accord with the cross-view SEM observation.

The water contact angle of the PVK film was measured to evaluate the hydrophobicity of the PVK films (Fig. 1f and 1i). Compared to the pristine PVK film, the Lanz-modified PVK films has a larger water contact angle, indicating an enhanced hydrophobicity of the PVK film after Lanz-modified, and leading to the improvement of environmental stability of the devices. The improved hydrophobicity of the PVK films can be ascribed to the hydrogen bond between the trifluoromethyl moiety on Lanz and FA⁺ and the coverage of – CF₃ group on the perovskite films.

Fig. 2a display the Fourier transform infrared (FTIR) spectra of the pristine and Lanz modified PVK films. Compared with the pristine PVK films, the N – H vibration peak of the Lanz-modified PVK film shifts to a lower band. This is due to the formation of the N – H···F hydrogen bond between FA⁺ cations and – CF₃ group in the Lanz-modified PVK film. The appearance of the hydrogen bond leads to the delocalization of the N – H bond electronic cloud, which weakens the N – H chemical bond energy, and then reduces the corresponding vibration frequency [33]. In order to confirm the existence of hydrogen bond between Lanz and PVK, liquid-state H NMR measurements were carried out and shown in Fig. S4. It can be noticed that the proton peaks in FA⁺ group shift to low filed after the incorporation of Lanz, manifesting the formation of hydrogen bonds between – CF₃ group and FA⁺ cations.

The compositions distribution of the device of FTO/SnO₂/PVK/spiro-OMeTAD was atomized by using the time of flight secondary-ion mass spectroscopy (TOF-SIMS) [34], and the results are demonstrated in Fig. 2b and 2c. The intensity of I₃⁻ in the Lanz-modified PVK film is

almost one order of magnitude lower than that in pristine PVK film, indicating a significant suppressed formation of iodine, which is responsible for the mitigated non-radiative recombination pathways. It could be observed that the distribution of F⁻ is mainly accumulated at the Lanz-doped PVK/HTL (hole transport layer) interfaces, suggesting Lanz molecules are predominantly concentrated at the surface rather than the bulk of PVK films, the results agree with the water contact angle observation, which is beneficial for the enhanced moisture resistance of the PSCs.

To verify the elimination effect of Pb⁰ and I⁰ defects by Lanz, we blended I₂ powder (30 mg) and metallic Pb powder (30 mg) into a mixed solution of isopropanol (IPA) and N, N-dimethylformamide (DMF) (volume ratio of 10:1) (Fig. 2d). Afterwards, Lanz (5 mg) was added to the experimental group, and then the mixed solution was heated at 100 °C for different times. It can be seen that with the heating time increase, the Lanz-added solution gradually change color from deep brown to light brown, accompanied with a small amount of particle precipitation. This precipitation was identified as lead iodide by X-ray diffraction (Fig. S5). These results demonstrate that Lanz can promote the formation of PbI₂, which may help to reduce the Pb⁰ and I⁰ defects within the PVK film [35,36].

X-ray photoelectron spectroscopy (XPS) in Pb 4f region of the pristine and Lanz-modified PVK films in different ripening times is revealed in Fig. 2e. Compared to the pristine PVK film, the peaks of Pb 4f shift to lower position in the Lanz-modified film, which is due to the interaction between Pb²⁺ and Lanz, and verifies that Lanz can passivate uncoordinated Pb²⁺ ions. On the other hand, with the increase of illumination time, the two small peaks of metallic lead (Pb⁰) in the pristine PVK film are identified, which could be caused by uncoordinated Pb²⁺ [37]. It is interesting to note that peaks of Pb⁰ is not observed in the Lanz-modified PVK film, demonstrating that Lanz can stabilize the perovskite

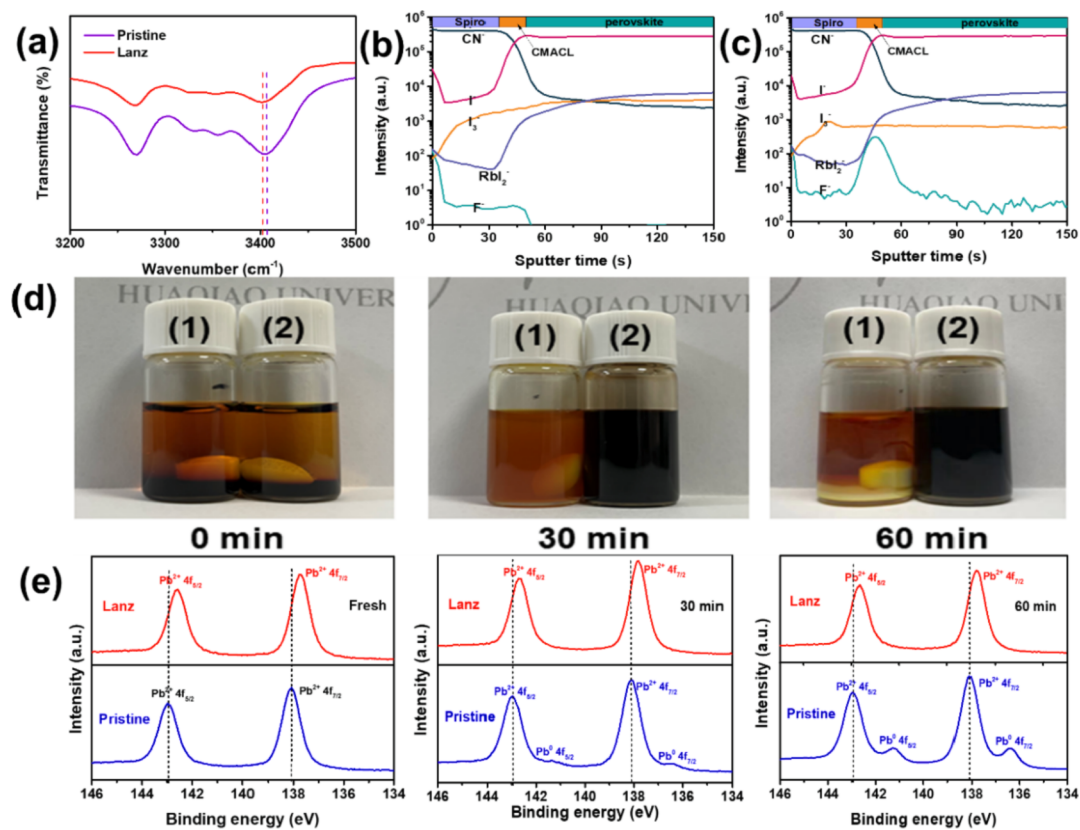


Fig. 2. (a) Fourier transform infrared (FTIR) spectra of pristine and Lanz-modified PVK films. (b, c) TOF-SIMS depth profile of pristine and Lanz-modified PVK films. (d) I₂ and Pb powder were dispersed in mixed DMF/IPA solvent (volume ratio 1:10) with Lanz (1) and without Lanz (2), which were stirred and heated at 100 °C for different times. (e) XPS spectra in Pb 4f region.

structure and has a positive effect for eliminating Pb^0 defects.

XPS spectra in C1s region of pristine and Lanz-modified PVK film is shown in Fig. S6. Obviously, the C – O intensity ratio [$\text{C} - \text{O}/(\text{C} - \text{O} + (\text{C} - \text{C}/\text{C} = \text{C}))$] in the Lanz-modified PVK film is lower than that of the pristine one, which indicates that Lanz restrains the decomposition of PVK and improved the stability of the film [38].

Kelvin probe force microscopy (KPFM) of PVK films was measured, and the results are shown in Fig. 3a and 3b. The Lanz-modified film shows a relatively uniform surface potential distribution compared with the pristine film. Furthermore, from the surface potential lines depicted in Fig. 3c, a 150 mV surface potential decrease from -300 to -150 mV is observed after Lanz modification, which coincides well with the water contact angle measurement.

Ultraviolet-visible (UV-vis) absorption spectra of pristine and Lanz-modified PVK films were measured and shown in Fig. S7. Clearly, a remarkable increase in the UV-vis absorption of Lanz-modified PVK film in the range of 300–550 nm in comparison with that of pristine one, ascribed to the improved film quality which is consistent with the results of XRD and SEM.

Ultraviolet Photoelectron Spectra (UPS) and angle-dependent hard X-ray photoelectron spectroscopy (AD-HAXPES) characterizations were measured [39]. From the UPS spectra shown in Fig. 3d, it can be observed that the work function (WF) and ionization potential (IP) of the pristine PVK film are 5.56 eV and 4.72 eV, respectively. After the introduction of Lanz, a 70 meV decrease in WF from 4.72 to 4.65 eV is noticed, and the value of IP is reduced from 5.56 to 5.41 eV [40].

Energy band diagram of the PVK with and without Lanz is depicted in Fig. 3e. The Fermi level position (EF) value relative to the valence band maximum (VBM) is changed from 0.84 to 0.76 eV, indicating that a

more p-type characteristic of the surface of PVK film after doping with Lanz. It can be seen that the introduction of Lanz can cause band-bending effect (Fig. 3f), contributing to quick hole-extraction from the PVK layer to HTL [41].

The steady-state photoluminescence (PL) and the time-resolved photoluminescence (TRPL) were characterized to investigate the carrier transport dynamics. As shown in Fig. 4a, the PL peak position of PVK film shifts from 797 to 793 nm after doping with Lanz. Moreover, the peak intensity of PL increases significantly with the addition of Lanz, hinting at a reduced non-radiative recombination, which is due to the decrease of trap states in the Lanz-modified PVK film. The time-resolved photoluminescence (TRPL) decay curve are shown in Fig. 4b. The TRPL curve is fitted by the formula: $I(t) = I_0 + A_1 e^{-t/\tau_1} + A_2 e^{-t/\tau_2} + y_0$ [42].

The corresponding carrier decay lifetime is calculated and listed in Table S1. The fast decay lifetime (τ_1) is ascribed to the non-radiative recombination caused by the defect at the interface between PVK and HTL, while the slow decay lifetime (τ_2) represents the radiative recombination before the charge collection [31]. It is worth noting that the decay lifetime of the Lanz-modified film is significantly longer than that of the pristine film. The τ_1 value increase from 13.93 to 27.02 ns, the τ_2 increases from 47.03 to 148.08 ns, and average photo-generated carrier lifetime (τ_{ave}) increase from 31.98 to 140.96 ns. The extension of decay lifetimes substantively confirm that Lanz can effectively passivate and alleviate defects on the interface and in the body, and reduces carrier non-radiative recombination [43]. This result is consistent with XPS characterization.

As further evidence, the transient photovoltage (TPV) decays curves of the devices under open-circuit were recorded and shown in Fig. 4c.

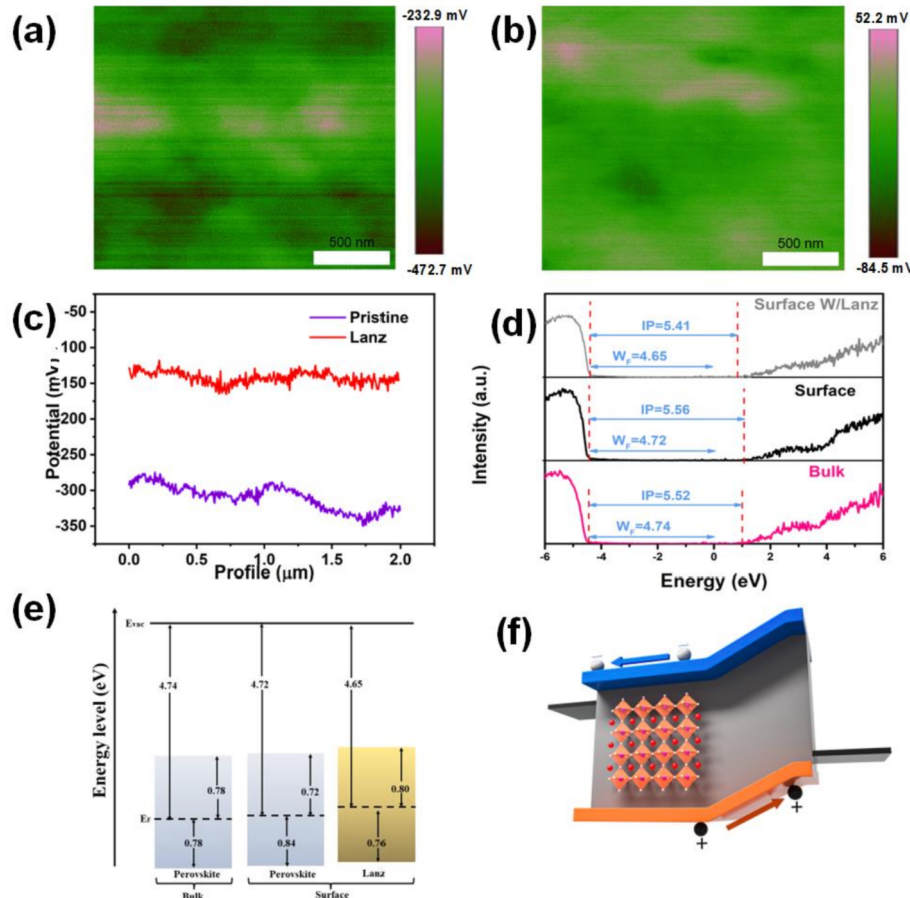


Fig. 3. (a, b) KPFM images, (c) Surface potential from KPFM of the pristine and Lanz-modified PVK films. (d) UPS spectra of the pristine and Lanz-modified PVK films. (e) Energy band diagram of the pristine and Lanz-modified PVK films. (f) Schematic diagram of the band-bending in the Lanz-modified PVK film.

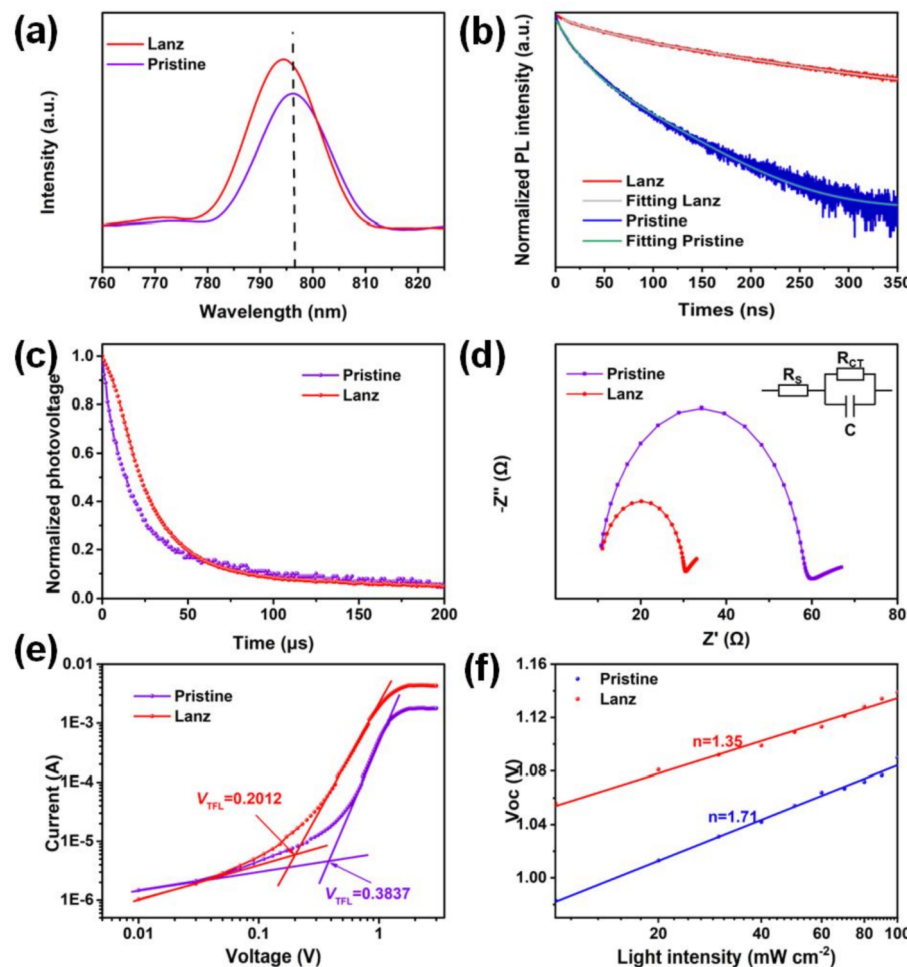


Fig. 4. (a) Steady-state photoluminescence (PL) spectra, (b) Time-resolved photoluminescence (TRPL) spectra of the pristine and Lanz-modified films. (c) Normalized TPV curves (d) Nyquist plots of the pristine and Lanz-modified devices. (e) Dark current–voltage curve of the devices with the hole-only structure of FTO/PEDOT/perovskite/spiro-OMeTAD/Au. (f) Dependency of V_{OC} on light intensity of the pristine and Lanz-modified devices.

The curve of the Lanz-modified devices exhibits a slightly longer decay lifetime than the pristine one, indicating the decrease of charge carrier recombination [44], which agrees with the TRPL results.

To evaluate the quality and damage interface effects of the PVSK films, PL mapping was recorded [37]. As shown in Fig. S8, and the brightness of the color bar corresponds to the relative value of PL intensity. It is obviously found that the luminescence intensity of the PVSK film on the plane scale is improved after Lanz modification, which is consistent with observation of the previous test results.

The electrochemical impedance spectroscopy (EIS) of the devices were collected to investigate the carrier transportation. As shown in Fig. 4d and Table S2, the device without Lanz displays the higher charge transfer resistance (R_{CT}), which signifies that the addition of Lanz is beneficial for carrier transportation and reduce interfacial potential barriers. The dark J-V curves of the devices are given in Fig. S9. Obviously, the Lanz-modified device exhibits a lower leakage current density than the pristine device, which further verifies that the introduction of Lanz can improve the charge carrier transportation in PSCs.

The density of trap states (N_t) in PVSK film were characterized by measuring the dark J-V curves of the hole-only devices (FTO/PEDOT:PSS/PVSK/spiro-OMeTAD/Au) using the space-charge-limited current (SCLC) model, and the results are shown in Fig. 4e. The trap-filled limit voltage (V_{TFL}) in pristine and Lanz-modified PVSK films can be calculated as 0.3837 and 0.2012 V, respectively. The corresponding density of trap states (N_t) are $5.52 \times 10^{15} \text{ cm}^{-3}$ and $2.89 \times 10^{15} \text{ cm}^{-3}$, respectively [45–47]. The results demonstrate that Lanz-treatment could efficiently

reduce density of trap states and improve the quality of PVSK film.

Decrease of density of trap states in Lanz-modified film was further verified by the characterization of thermal admittance spectroscopy (TAS) [48,49]. The related results are plotted in Figure S10. The density of defect states of pristine device is relatively large, which accounts for the current hysteresis phenomenon under light conditions. The introduction of Lanz in the PVSK film also reduces the tDOS of the band with an energy level higher than 0.56 eV by nearly two orders of magnitude. The significant reduction in tDOS is consistent with the mitigation in the photocurrent hysteresis, which indicates that the introduction of Lanz could passivate deep level defects in the PVSK films.

To investigate the recombination mechanism of the PSCs, the light-intensity-dependent open circuit voltage (V_{OC}) of PSC device was carried out. Fig. 4f depicts the relationship between light intensity (I) and V_{OC} . Compared with the ideal factor based on pristine device (1.71), the value of the device modified with Lanz is 1.35, indicating that bimolecular recombination is effectively suppressed by Lanz-modification [50,51].

Under simulated sunlight illumination with intensity of 100 mW cm^{-2} (AM 1.5 G), the J-V curves of the devices modified with different Lanz concentrations were measured and recorded in Fig. 5a, and the photovoltaic parameters are listed in Table S3. With the increase of the Lanz concentrations doped in PVSK film, the photovoltaic performance of the device enhances compared with the pristine device. When the doped Lanz concentration reaches 0.1 mol. %, the PSC achieves the excellently power conversion efficiency (PCE) of 24.05%, together with

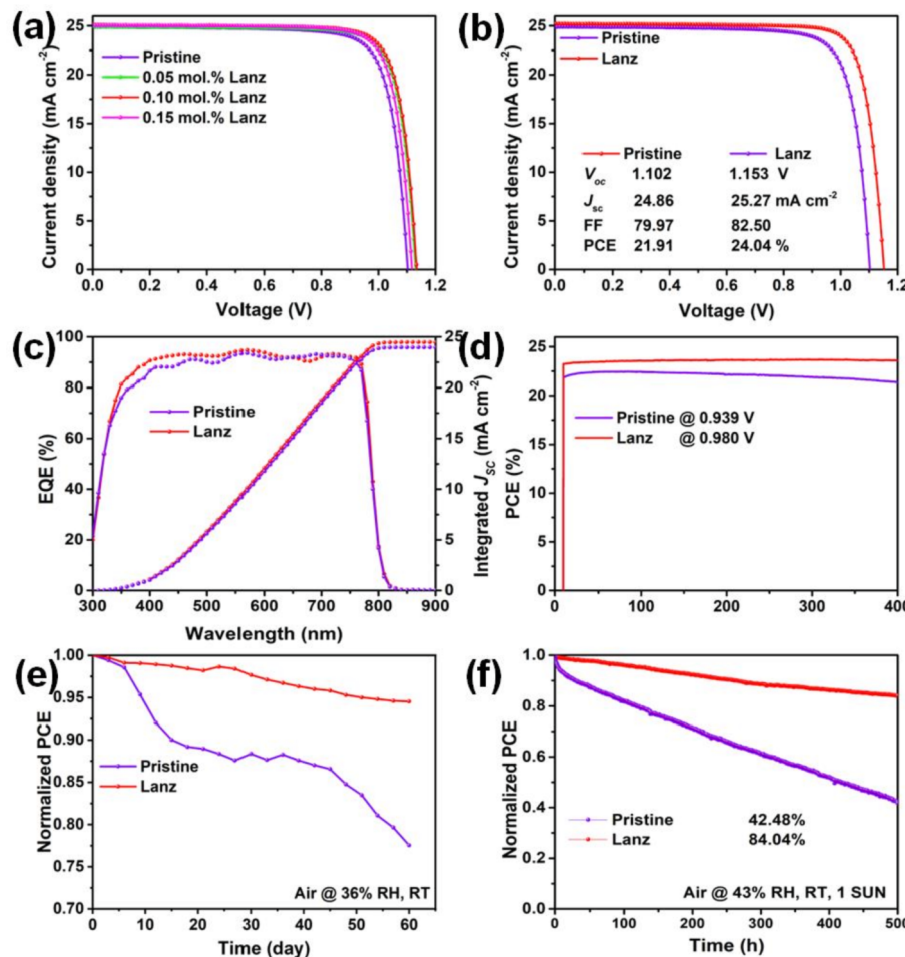


Fig. 5. (a) J - V curves of the devices modified with different Lanz concentrations. (b) J - V curves of the PSCs. (c) EQE and integrated J_{SC} curves of the pristine and Lanz-modified devices. (d) Steady-state power output at maximum power point (MPPT) of devices. (e) Environmental stability test. (f) Operational stability test of the unencapsulated devices.

a V_{OC} of 1.153 V, a short-circuit current density (J_{SC}) of 25.28 mA cm^{-2} , and a fill factor (FF) of 82.50%. Obviously, the increased PCE of Lanz-based device is mainly derived from the enlargement of V_{OC} , implying a significant suppression of non-radiative carrier recombination, which agrees well with the consequences of characterization measurements aforementioned (e.g., PL, TRPL, TAS, TPV and so on). When the concentration of Lanz is 0.15 mol. %, the PCE of the device decreases from 24.05% to 22.75%. Typical comparative photovoltaic curves and parameters are described in Fig. 5b.

Fig. 5c depicts the external quantum efficiency (EQE) and integrated J_{SC} curves of the devices with or without Lanz-modification. Compared with the pristine device, the Lanz-modified device shows a higher EQE value in the spectral range from 350 to 550 nm, which is in accordance with the increased UV-vis light absorption spectra of Lanz-modified PVK film in the range of 350–550 nm. The integrated J_{SC} values of the devices are summarized on Table S4. The integrated J_{SC} of pristine and Lanz-modified device is 23.97 and 24.47 mA cm^{-2} , respectively. These result basically consistent with the results of J - V curves. The steady-state power output (SPO) characteristics at the maximum power point (MPPT) of devices were record in Fig. 5d. It is obviously found that the device has a higher stabilized PCE after Lanz-modification.

To check the reproducibility and reliability of the performance of device, we parallelly tested photovoltaic parameters of the pristine and Lanz-modified devices a batch of 15, respectively. The related statistical results are listed in Fig. S11. The Lanz-modified devices exhibit a highly concentrated parameter distribution, indicating a wonderful

reproducibility.

The hysteresis behaviors of the devices were estimated by recording the J - V curves in different scanning direction. The hysteresis index (HI) is defined as: $HI = \frac{PCE_{RS} - PCE_{ES}}{PCE_{RS}}$ [52,53]. As shown in Fig. S12 and Table S5. The pristine device has an HI value of 0.080. However, after Lanz-treatment the modified device presents a negligible HI value of 0.026. This may be due to the fact that the introduced Lanz passivates defects and produces band bending, which is conducive to the migration of carriers.

Fig. S13 displays the photographs of pristine and Lanz-modified PVSK films stored in ambient air with relative humidity (RH) 60% for 60 days. It can be seen that after 36 days of storage, the color of the pristine film has become transparent, while the color of the modified film is basically unchanged; After 60 days, the pristine film was completely bleached, while the modified film has lighter color. Compared to the pristine films, the Lanz-modified films exhibit superior stability. The superior stability for Lanz-modified film is due to the formation of hydrogen bond between the trifluoromethyl moiety on Lanz and FA^+ on perovskite and strong hydrophobic groups ($-\text{CF}_3$) group covered atop the PVSK film, which consolidate the crystal structure of PVSK, and build a moisture-barrier to inhibit the decomposition of PVSK.

The environment stability of the PSCs was examined by measuring the PCEs of the unencapsulated devices stored in a dark under RH 36% at room temperature. The results were shown in Fig. 5e, after 60 days storage the pristine device keeps about 74% of its initial PCE, while the

Lanz-modified device maintains about 95% of its initial value, respectively. The operational stability of the devices was assessed by recording the PCE of the encapsulated devices under an illumination of Newport ABB class solar simulator (AM 1.5G) in air [54–56]. As represented in Fig. 5f, the Lanz-modified device maintains about 84.04% of its original efficiency after continuous one-sun illumination for 500 h. However, the pristine device decreases to around 60% of initial value. The excellent environmental and operational stability of the modified devices results from the superior stability for Lanz-modified films, which also further demonstrates the multiple effects of introduction of Lanz.

3. Conclusion

In summary, as a multifunctional additive rather than medicine, Lansoprazole (Lanz) is introduced into the perovskite photo-absorber layer. The electron-donating sulfinyl moiety ($>S = O$) on Lanz coordinate with empty orbit of Pb^{2+} ions, which passivates the defects on the interface and in the bulk of PVK, minimizes carrier non-radiative recombination and improves the performance of PSCs. The introduction of Lanz retards the growth rate of perovskite, improves crystal quality and reduce grain boundaries and defects, which contribute to imporve the device performance. The modification of Lanz tune the Fermi-level of perovskite film and cause surface band-bending effect, which unhindereds the separation, extraction and transportation of carriers. The strong hydrophobic trifluoromethyl group ($-CF_3$) on Lanz cover atop of perovskite through hydrogen bond interaction, which hinder the intrudion vasion of moiture and oxygen, enhance the stability of device. The multi-functional cooperation of Lanz enables perovskite solar cells a superior performance. Compared to the pristine device of PCE of 21.91%, the Lanz-modified device acquires a excellent PCE of 24.05%, together with outstanding environmental and operational stability.

Declaration of Competing Interest

The authors declare that they have no known competing financial interests or personal relationships that could have appeared to influence the work reported in this paper.

Acknowledgement

The authors are grateful to the financial support from the National Natural Science Foundation of China (Nos. 51972123, U1705256, 61804058).

Appendix A. Supplementary data

Supplementary data to this article can be found online at <https://doi.org/10.1016/j.cej.2022.137416>.

References

- [1] Best research-cell efficiencies chart. <https://www.nrel.gov/pv/assets/pdfs/best-research-cell-efficiencies-rev220126.pdf>, 2022 (accessed 26 January 2022).
- [2] A. Kojima, K. Teshima, Y. Shirai, T. Miyasaka, Organometal halide perovskites as visible-light sensitizers for photovoltaic cells, *J. Am. Chem. Soc.* 131 (2009) 6050–6051, <https://doi.org/10.1021/ja809598r>.
- [3] H.S. Kim, C.R. Lee, J.H. Im, K.B. Lee, T. Moehl, A. Marchioro, S.J. Moon, R. Humphry-Baker, J.H. Yum, J.E. Moser, M. Gratzel, N.G. Park, Lead iodide perovskite sensitized all-solid-state submicron thin film mesoscopic solar cell with efficiency exceeding 9%, *Sci. Rep.* 2 (2012) 591, <https://doi.org/10.1038/srep00591>.
- [4] M.M. Lee, J. Teuscher, T. Miyasaka, T.N. Murakami, H.J. Snaith, Efficient hybrid solar cells based on meso-superstructured organometal halide perovskites, *Science* 338 (2012) 643–647, <https://doi.org/10.1126/science.1228604>.
- [5] M.A. Green, A. Ho-Baillie, H.J. Snaith, The emergence of perovskite solar cells, *Nat. Photonics* 8 (2014) 506–514, <https://doi.org/10.1038/nphoton.2014.134>.
- [6] H.J. Snaith, Perovskites: the emergence of a new era for low-cost, high-efficiency solar cells, *The Journal of Physical Chemistry Letters* 4 (2013) 3623–3630, <https://doi.org/10.1021/jz4020162>.
- [7] S. Wang, F. Cao, Y. Wu, X. Zhang, J. Zou, Z. Lan, W. Sun, J. Wu, P. Gao, Multifunctional 2D perovskite capping layer using cyclohexylmethylenammonium bromide for highly efficient and stable perovskite solar cells, *Mater. Today Phys.* 21 (2021), 100543, <https://doi.org/10.1016/j.mtphys.2021.100543>.
- [8] J.A. Christians, P. Schulz, J.S. Tinkham, T.H. Schloemer, S.P. Harvey, B.J. Tremolet de Villiers, A. Sellinger, J.J. Berry, J.M. Luther, Tailored interfaces of unencapsulated perovskite solar cells for >1,000 hour operational stability, *Nat. Energy* 3 (2018) 68–74, <https://doi.org/10.1038/s41560-017-0067-y>.
- [9] Q. Dong, C. Zhu, M. Chen, C. Jiang, J. Guo, Y. Feng, Z. Dai, S.K. Yadavalli, M. Hu, X. Cao, Y. Li, Y. Huang, Z. Liu, Y. Shi, L. Wang, N.P. Padture, Y. Zhou, Interpenetrating interfaces for efficient perovskite solar cells with high operational stability and mechanical robustness, *Nat. Commun.* 12 (2021) 973, <https://doi.org/10.1038/s41467-021-21292-3>.
- [10] N. Li, X. Niu, Q. Chen, H. Zhou, Towards commercialization: the operational stability of perovskite solar cells, *Chem. Soc. Rev.* 49 (2020) 8235–8286, <https://doi.org/10.1039/d0cs00573h>.
- [11] W. Nie, H. Tsai, R. Asadpour, J.C. Blancon, A.J. Neukirch, G. Gupta, J.J. Crochet, M. Chhowalla, S. Tretiak, M.A. Alam, H.L. Wang, A.D. Mohite, High-efficiency solution-processed perovskite solar cells with millimeter-scale grains, *Science* 347 (2015) 522–525, <https://doi.org/10.1126/science.aaa0472>.
- [12] E. Aydin, M. De Bastiani, S. De Wolf, Defect and Contact Passivation for Perovskite Solar Cells, *Adv. Mater.* 31 (2019) e1900428. <https://doi.org/10.1002/adma.201900428>.
- [13] Y. Shao, Y. Fang, T. Li, Q. Wang, Q. Dong, Y. Deng, Y. Yuan, H. Wei, M. Wang, A. Griverman, J. Shield, J. Huang, Grain boundary dominated ion migration in polycrystalline organic-inorganic halide perovskite films, *Energy Environ. Sci.* 9 (2016) 1752–1759, <https://doi.org/10.1039/c6ee00413j>.
- [14] F. Gao, Y. Zhao, X. Zhang, J. You, Additive engineering for efficient and stable perovskite solar cells, *Adv. Energy Mater.* 10 (2019) 1902579, <https://doi.org/10.1002/aenm.201902579>.
- [15] X. Zhou, W. Qi, J. Li, J. Cheng, Y. Li, J. Luo, M.J. Ko, Y. Li, Y. Zhao, X. Zhang, Toward efficient and stable perovskite solar cells: choosing appropriate passivator to specific defects, *Sol. RRL* 4 (2020) 2000308, <https://doi.org/10.1002/solr.202000308>.
- [16] X. Xia, J. Peng, Q. Wan, X. Wang, Z. Fan, J. Zhao, F. Li, Functionalized ionic liquid-crystal additive for perovskite solar cells with high efficiency and excellent moisture stability, *ACS Appl. Mater. Interfaces* 13 (2021) 17677–17689, <https://doi.org/10.1021/acsmami.1c02728>.
- [17] J. Xie, K. Yan, H. Zhu, G. Li, H. Wang, H. Zhu, P. Hang, S. Zhao, W. Guo, D. Ye, L. Shao, X. Guan, T. Ngai, X. Yu, J. Xu, Identifying the functional groups effect on passivating perovskite solar cells, *Sci. Bull.* 65 (2020) 1726–1734, <https://doi.org/10.1016/j.scib.2020.05.031>.
- [18] Z. Guo, T. Gao, J. Zhuang, X. Liu, H. Guo, J. Yi, Z. Ma, H. Li, X. Cheng, Synergistic defect passivation for highly efficient and stable perovskite solar cells using sodium dodecyl benzene sulfonate, *ACS Appl. Energy Mater.* 4 (2021) 4910–4918, <https://doi.org/10.1021/acsaem.1c00502>.
- [19] L. Yang, Q. Xiong, Y. Li, P. Gao, B. Xu, H. Lin, X. Li, T. Miyasaka, Artemisinin-passivated mixed-cation perovskite films for durable flexible perovskite solar cells with over 21% efficiency, *J. Mater. Chem. A* 9 (2021) 1574–1582, <https://doi.org/10.1039/d0ta10717d>.
- [20] P. Zhang, F. Cao, W. Tian, L. Li, Thiamine additive engineering enables improved film formation towards high efficiency and moisture stability in perovskite solar cells, *Sci. China Mater.* 65 (2) (2022) 321–327.
- [21] Y. Hou, K. Wang, D. Yang, Y. Jiang, N. Yennawar, K. Wang, M. Sanghadasa, C. Wu, S. Priya, Enhanced performance and stability in DNA-perovskite heterostructure-based solar cells, *ACS Energy Lett.* 4 (2019) 2646–2655, <https://doi.org/10.1021/acsenergylett.9b01894>.
- [22] R. Wang, J. Xue, L. Meng, J.-W. Lee, Z. Zhao, P. Sun, L. Cai, T. Huang, Z. Wang, Z.-K. Wang, Y. Duan, J.L. Yang, S. Tan, Y. Yuan, Y. Huang, Y. Yang, Caffeine improves the performance and thermal stability of perovskite solar cells, *Joule* 3 (2019) 1464–1477, <https://doi.org/10.1016/j.joule.2019.04.005>.
- [23] Y. Hou, C. Wu, D. Yang, K. Wang, T. Ye, L. Brownlie, K. Wang, S. Priya, Artemisinin (ART)-Induced “perovskite/perovskite” bilayer structured photovoltaics, *Nano Energy* 78 (2020), 105133, <https://doi.org/10.1016/j.nanoen.2020.105133>.
- [24] Q. Zhang, J. Duan, Q. Guo, J. Zhang, D. Zheng, F. Yi, X. Yang, Y. Duan, Q. Tang, Thermal-triggered dynamic disulfide bond self-heals inorganic perovskite solar cells, *Angew. Chem. Int. Ed.* 61 (2022) e202116632.
- [25] T. Iwahashi, H. Satoh, M. Nakao, T. Iwasaki, T. Yamazaki, K. Kubo, T. Tamura, A. Imada, Lansoprazole, a novel benzimidazole proton pump inhibitor, and its related compounds have selective activity against Helicobacter pylori, *Antimicrob. Agents Chemother.* 35 (1991) 490–496, <https://doi.org/10.1128/AAC.35.3.490>.
- [26] R. Eissele, G. Brunner, B. Simon, E. Solcia, R. Arnold, Gastric mucosa during treatment with lansoprazole: Helicobacter pylori is a risk factor for argyrophil cell hyperplasia, *Gastroenterology* 112 (1997) 707–717, <https://doi.org/10.1053/gast.1997.v112.pm14041231>.
- [27] K.C. Lai, S.K. Lam, K.M. Chu, W.M. Hui, K.F. Kwok, B.C. Wong, H.C. Hu, W. M. Wong, O.O. Chan, C.K. Chan, Lansoprazole reduces ulcer relapse after eradication of Helicobacter pylori in nonsteroidal anti-inflammatory drug users—a randomized trial, *Aliment. Pharmacol. Ther.* 18 (2003) 829–836, <https://doi.org/10.1046/j.1365-2036.2003.01762.x>.
- [28] M. Vatanparast, Z. Sharifiinia, Isoindigo derivatives as promising hole transport materials for perovskite solar cells, *Sol. Energy* 230 (2021) 260–268, <https://doi.org/10.1016/j.solener.2021.10.049>.
- [29] X. Zheng, B. Chen, J. Dai, Y. Fang, Y. Bai, Y. Lin, H. Wei, X.C. Zeng, J. Huang, Defect passivation in hybrid perovskite solar cells using quaternary ammonium

- halide anions and cations, *Nat. Energy.* 2 (2017) 17102, <https://doi.org/10.1038/nenergy.2017.102>.
- [30] H. Kanda, N. Shibayama, A.J. Huckaba, Y. Lee, S. Paek, N. Klipfel, C. Roldán-Carmona, V.I.E. Queloz, G. Grancini, Y. Zhang, M. Abuhelaiqa, K.T. Cho, M. Li, M. D. Mensi, S. Kinge, M.K. Nazeeruddin, Band-bending induced passivation: high performance and stable perovskite solar cells using a perhydropoly(silazane) precursor, *Energy Environ. Sci.* 13 (2020) 1222–1230, <https://doi.org/10.1039/c9ee02028d>.
- [31] J. Jia, J. Dong, B. Shi, J. Wu, Y. Wu, B. Cao, Postpassivation of $\text{Cs}_{0.05}(\text{FA}_{0.17})_{0.95}\text{Pb}(\text{I}_{0.83}\text{Br}_{0.17})_3$ Perovskite Films with Tris(pentafluorophenyl)-borane, *ACS Appl Mater. Interfaces.* 13 (2021) 2472–2482, <https://doi.org/10.1021/acsami.0c16939>.
- [32] J. Dong, J. Jia, X. Feng, B. Shi, Y. Wu, Y. Zhang, J. Wu, B. Cao, Ligand exchange of SnO_2 effectively improving the efficiency of flexible perovskite solar cells, *J. Alloys Compd.* 883 (2021), 160827, <https://doi.org/10.1016/j.jallcom.2021.160827>.
- [33] N. Li, S. Tao, Y. Chen, X. Niu, C.K. Onwudinanti, C. Hu, Z. Qiu, Z. Xu, G. Zheng, L. Wang, Y. Zhang, L. Li, H. Liu, Y. Lun, J. Hong, X. Wang, Y. Liu, H. Xie, Y. Gao, Y. Bai, S. Yang, G. Brocks, Q. Chen, H. Zhou, Cation and anion immobilization through chemical bonding enhancement with fluorides for stable halide perovskite solar cells, *Nat. Energy.* 4 (2019) 408–415, <https://doi.org/10.1038/s41560-019-0382-6>.
- [34] S.P. Harvey, J. Messinger, K. Zhu, J.M. Luther, J.J. Berry, Investigating the effects of chemical gradients on performance and reliability within perovskite solar cells with TOF-SIMS, *Adv. Energy Mater.* 10 (2020) 1903674, <https://doi.org/10.1002/aenm.201903674>.
- [35] L. Wang, H. Zhou, J. Hu, B. Huang, M. Sun, B. Dong, G. Zheng, Y. Huang, Y. Chen, L. Li, Z. Xu, N. Li, Z. Liu, Q. Chen, L.D. Sun, C.H. Yan, A Eu(3+)-Eu(2+) ion redox shuttle imparts operational durability to Pb-I perovskite solar cells, *Science* 363 (2019) 265–270, <https://doi.org/10.1126/science.aau5701>.
- [36] J. Dou, C. Zhu, H. Wang, Y. Han, S. Ma, X. Niu, N. Li, C. Shi, Z. Qiu, H. Zhou, Y. Bai, Q. Chen, Synergistic Effects of Eu-MOF on Perovskite Solar Cells with Improved Stability, *Adv. Mater.* 33 (2021) e2102947. <https://doi.org/10.1002/adma.202102947>.
- [37] Y. Wang, X. Wang, C. Wang, R. Cheng, L. Zhao, X. Wang, X. Zhang, J. Shang, H. Zhang, L. Zhao, Y. Tu, W. Huang, Defect suppression and energy level alignment in formamidinium-based perovskite solar cells, *J. Energy Chem.* 67 (2022) 65–72, <https://doi.org/10.1016/j.jec.2021.09.043>.
- [38] Z. Zhang, Y. Gao, Z. Li, L. Qiao, Q. Xiong, L. Deng, Z. Zhang, R. Long, Q. Zhou, Y. Du, Z. Lan, Y. Zhao, C. Li, K. Mullen, P. Gao, Marked Passivation Effect of Naphthalene-1,8-Dicarboximides in High-Performance Perovskite Solar Cells, *Adv. Mater.* 33 (2021) e2008405. <https://doi.org/10.1002/adma.202008405>.
- [39] Q. Cao, J. Yang, T. Wang, Y. Li, X. Pu, J. Zhao, Y. Zhang, H. Zhou, X. Li, X. Li, Star-polymer multidentate-cross-linking strategy for superior operational stability of inverted perovskite solar cells at high efficiency, *Energy Environ. Sci.* 14 (2021) 5406–5415, <https://doi.org/10.1039/dlee01800k>.
- [40] S. Xiong, Z. Hou, S. Zou, X. Lu, J. Yang, T. Hao, Z. Zhou, J. Xu, Y. Zeng, W. Xiao, W. Dong, D. Li, X. Wang, Z. Hu, L. Sun, Y. Wu, X. Liu, L. Ding, Z. Sun, M. Fahlman, Q. Bao, Direct Observation on p- to n-Type Transformation of Perovskite Surface Region during Defect Passivation Driving High Photovoltaic Efficiency, *Joule.* 5 (2021) 467–480, <https://doi.org/10.1016/j.joule.2020.12.009>.
- [41] Q. Guo, X. Yang, Y. Wang, W. Xu, J. Duan, Q. Tang, Dielectric Hole Collector toward Boosting Charge Transfer of CsPbBr₃ Hybrid Nanogenerator by Coupling Triboelectric and Photovoltaic Effects, *Adv. Funct. Mater.* 31 (2021) 2101348, <https://doi.org/10.1002/adfm.202101348>.
- [42] C. Liu, S. Liu, Y. Wang, Y. Chu, K. Yang, X. Wang, C. Gao, Q. Wang, J. Du, S. Li, Y. Hu, Y. Rong, L. Guo, A. Mei, H. Han, Improving the Performance of Perovskite Solar Cells via a Novel Additive of N,1-Fluoroformamidinium Iodide with Electron-
- Withdrawing Fluorine Group, *Adv. Func. Mater.* 31 (2021) 2010603, <https://doi.org/10.1002/adfm.202010603>.
- [43] X. Wang, J. Wu, Y. Yang, X. Liu, Q. Guo, Z. Song, G. Li, Z. Lan, M. Huang, High performance and stable perovskite solar cells using vanadic oxide as a dopant for spiro-OMeTAD, *J. Mater. Chem. A.* 7 (2019) 13256–13264, <https://doi.org/10.1039/c9ta03351c>.
- [44] Q. Xiong, L. Yang, Q. Zhou, T. Wu, C.L. Mai, Z. Wang, S. Wu, X. Li, P. Gao, NdCl₃ Dose as a Universal Approach for High-Efficiency Perovskite Solar Cells Based on Low-Temperature-Processed SnO_x, *ACS Appl. Mater. Interfaces.* 12 (2020) 46306–46316, <https://doi.org/10.1021/acsami.0c13296>.
- [45] T. Niu, J. Lu, M.-C. Tang, D. Barrat, D.-M. Smilgies, Z. Yang, J. Li, Y. Fan, T. Luo, I. McCulloch, A. Amassian, S. Liu, K. Zhao, High performance ambient-air-stable FAPbI₃ perovskite solar cells with molecule-passivated Ruddlesden-Popper/3D heterostructured film, *Energy Environ. Sci.* 11 (2018) 3358–3366, <https://doi.org/10.1039/c8ee02542h>.
- [46] R. Azmi, S.-H. Oh, S.-Y. Jang, High-Efficiency Colloidal Quantum Dot Photovoltaic Devices Using Chemically Modified Heterojunctions, *ACS Energy Lett.* 1 (2016) 100–106, <https://doi.org/10.1021/acsenergylett.6b00070>.
- [47] Y. Tu, X. Yang, R. Su, D. Luo, Y. Cao, L. Zhao, T. Liu, W. Yang, Y. Zhang, Z. Xu, Q. Liu, J. Wu, Q. Gong, F. Mo, R. Zhu, Diboron-Assisted Interfacial Defect Control Strategy for Highly Efficient Planar Perovskite Solar Cells, *Adv. Mater.* 30 (2018) e1805085. <https://doi.org/10.1002/adma.201805085>.
- [48] Y. Shao, Z. Xiao, C. Bi, Y. Yuan, J. Huang, Origin and elimination of photocurrent hysteresis by fullerene passivation in $\text{CH}_3\text{NH}_3\text{PbI}_3$ planar heterojunction solar cells, *Nat. Commun.* 5 (2014) 5784, <https://doi.org/10.1038/ncomms6784>.
- [49] S. Khelifi, K. Decock, J. Lauwaert, H. Vrielinck, D. Spolteore, F. Piersimon, J. Manca, A. Belghachi, M. Burgelman, Investigation of defects by admittance spectroscopy measurements in poly (3-hexylthiophene):(6,6)-phenyl C61-butyric acid methyl ester organic solar cells degraded under air exposure, *J. Appl. Phys.* 110 (9) (2011) 094509.
- [50] F. Cai, J. Cai, L. Yang, W. Li, R.S. Gurney, H. Yi, A. Iraqi, D. Liu, T. Wang, Molecular engineering of conjugated polymers for efficient hole transport and defect passivation in perovskite solar cells, *Nano Energy* 45 (2018) 28–36, <https://doi.org/10.1016/j.nanoen.2017.12.028>.
- [51] X. Wang, J. Wu, Y. Yang, G. Li, Z. Song, X. Liu, W. Sun, Z. Lan, P. Gao, Chromium trioxide modified spiro-OMeTAD for highly efficient and stable planar perovskite solar cells, *J. Energy Chem.* 61 (2021) 386–394, <https://doi.org/10.1016/j.jec.2021.03.047>.
- [52] R. Sanchez, V. Gonzalez-Pedro, J. Lee, N. Park, Y. Kang, I. Mora-Sero, J. Bisquert, Slow Dynamical Processes in Lead Halide Perovskite Solar Cells. Characteristic Times and Hysteresis, *J. Phys. Chem. Lett.* 5 (2014) 2357–2363, <https://doi.org/10.1021/jz5011187>.
- [53] T.J. Jacobsson, J.P. Correa-Baena, E. Halvani Anaraki, B. Philippe, S.D. Stranks, M. E. Bouduban, W. Tress, K. Schenk, J. Teuscher, J.E. Moser, H. Rensmo, A. Hagfeldt, Unreacted PbI₂ as a Double-Edged Sword for Enhancing the Performance of Perovskite Solar Cells, *J. Am. Chem. Soc.* 138 (2016) 10331–10343, <https://doi.org/10.1021/jacs.b606320>.
- [54] Q. Xiong, C. Wang, Q. Zhou, L. Wang, X. Wang, L. Yang, J. Ding, C. Chen, J. Wu, X. Li, P. Gao, Rear Interface Engineering to Suppress Migration of Iodide Ions for Efficient Perovskite Solar Cells with Minimized Hysteresis, *Adv. Funct. Mater.* 32 (2021) 2107823, <https://doi.org/10.1002/adfm.202107823>.
- [55] B. Cai, Y. Xing, Z. Yang, W. Zhang, J. Qiu, High performance hybrid solar cells sensitized by organolead halide perovskites, *Energy Environ. Sci.* 6 (2013) 1480–1485, <https://doi.org/10.1039/c3ee40343b>.
- [56] J. Du, J. Duan, X. Yang, Y. Duan, Q. Zhou, Q. Tang, p-Type Charge Transfer Doping of Graphene Oxide with $(\text{NiCo})_{1-y}\text{Fe}_y\text{O}_x$ for Air-Stable, All-Inorganic CsPbI₃ Perovskite Solar Cells, *Angew. Chem. Int. Ed.* 60 (2021) 10608–10613, <https://doi.org/10.1002/anie.202016703>.